Multimode interference demultiplexers and splitters in metal-insulator-metal waveguides

Yao Kou and Xianfeng Chen*

Department of Physics, The State Key Laboratory on Fiber Optic Local Area Communication Networks and Advanced Optical Communication Systems, Shanghai Jiao Tong University, Shanghai 200240, China
*xfchen@sjtu.edu.cn

Abstract: Multimode interference (MMI) effect in metal-insulator-metal (MIM) waveguides is studied in this paper. Theoretical calculation based on the self-imaging principle and the finite element method (FEM) simulation are used to analyze the effect and further guide the design of plasmonic MMI devices. We show that wavelength-selective routing and splitting with high extinction ratios can be realized in the multimode waveguides, and active control by refractive index modulation is also demonstrated.

©2011 Optical Society of America

References and links

1. P. Berini, "Plasmon-polariton modes guided by a metal film of finite width bounded by different dielectrics," Opt. Express **7**(10), 329–335 (2000).
2. T. Holmgaard, and S. Bozhevolnyi, "Theoretical analysis of dielectric-loaded surface plasmon-polariton waveguides," Phys. Rev. B **75**(24), 245405 (2007).
3. A. Krasavin, and A. Zayats, "Three-dimensional numerical modeling of photonic integration with dielectric-loaded SPP waveguides," Phys. Rev. B **78**(4), 045425 (2008).
4. J. C. Weeber, A. Dereux, C. Girard, J. R. Krenn, and J. P. Goudonnet, "Plasmon polaritons of metallic nanowires for controlling submicron propagation of light," Phys. Rev. B **60**(12), 9061–9068 (1999).
5. H. Ditlbacher, A. Hohenau, D. Wagner, U. Kreibig, M. Rogers, F. Hofer, F. R. Aussenegg, and J. R. Krenn, "Silver nanowires as surface plasmon resonators," Phys. Rev. Lett. **95**(25), 257403 (2005).
6. R. Zia, M. D. Selker, P. B. Catrysse, and M. L. Brongersma, "Geometries and materials for subwavelength surface plasmon modes," J. Opt. Soc. Am. A **21**(12), 2442–2446 (2004).
7. J. Dionne, L. Sweatlock, H. Atwater, and A. Polman, "Plasmon slot waveguides: Towards chip-scale propagation with subwavelength-scale localization," Phys. Rev. B **73**(3), 035407 (2006).
8. L. B. Soldano, and E. C. M. Pennings, "Optical Multi-Mode Interference Devices Based on Self-Imaging: Principles and Applications," J. Lightwave Technol. **13**(4), 615–627 (1995).
9. J. Leuthold, J. Eckner, E. Gamper, P. A. Besse, and H. Melchior, "Multimode Interference Couplers for the Conversion and Combining of Zero- and First-Order Modes," J. Lightwave Technol. **16**(7), 1228–1239 (1998).
10. Y. J. Tsai, A. Degiron, N. M. Jokerst, and D. R. Smith, "Plasmonic multi-mode interference couplers," Opt. Express **17**(20), 17471–17482 (2009).
11. G. Yuan, P. Wang, Y. Lu, and H. Ming, "Multimode interference splitter based on dielectric-loaded surface plasmon polariton waveguides," Opt. Express **17**(15), 12594–12600 (2009).
12. I. P. Kaminow, W. L. Mammel, and H. P. Weber, "Metal-clad optical waveguides: analytical and experimental study," Appl. Opt. **13**(2), 396–405 (1974).
13. E. D. Palik, *Handbook of Optical Constants of Solids*, (Academic Press, Inc., 1985).
14. G. Veronis, and S. Fan, "Bends and splitters in metal-dielectric-metal subwavelength plasmonic waveguides," Appl. Phys. Lett. **87**(13), 131102 (2005).
15. T. D. Kim, J. Luo, J. W. Ka, S. Hau, Y. Tian, Z. Shi, N. M. Tucker, S. H. Jang, J. W. Kang, and A. K.-Y. Jen, "Ultralarge and Thermally Stable Electro-optic Activities from Diels-Alder Crosslinkable Polymers Containing Binary Chromophore Systems," Adv. Mater. (Deerfield Beach Fla.) **18**(22), 3038–3042 (2006).
16. E. M. McKenna, A. S. Lin, A. R. Mickelson, R. Dinu, and D. Jin, "Comparison of r33 values for AJ404 films prepared with parallel plate and corona poling," J. Opt. Soc. Am. B **24**(11), 2888–2892 (2007).

1. Introduction

Surface plasmon is regarded as a promising candidate for realizing chip-scale photonic integration and optical-electrical interconnection. To achieve this goal, several kinds of plasmonic waveguide-based structures, such as long range surface plasmon waveguides, dielectric-loaded waveguides, metallic nanowires and metal-insulator-metal (MIM) waveguides, have been proposed in the recent years [1–7], Among these, MIM waveguide

shows a special advantage for high-density integration, because it confines most of field in the insulator layer and then helps to reduce the devices size. As a tradeoff, its initial loss is also significant [6,7]

Recent advances in multimode dielectric waveguides show a great application value of multimode interference (MMI) effects in conventional integrated optics [8,9]. However, for the MIM waveguides, researches are generally focused on single mode waveguides which have the ability to guide and modulate light in a subwavelength scale, whereas very little attention has been paid on designing the plasmonic MMI devices. Recently, MMI splitters based on long-range surface plasmon waveguides or dielectric-loaded waveguides have been demonstrated, which show similar properties with the dielectric waveguides [10,11]. Since the wavelength division multiplexing system (WDM) requires various functional devices, it is important to explore the MMI effect and its application in different kinds of plasmonic waveguides.

In this paper, MMI effect in MIM waveguides is studied by theoretical calculation and finite element method (FEM) simulation (using COMSOL Multiphysics). With the help of the self-imaging principle, the interference property is analyzed, followed by a discussion of the plasmonic MMI devices, including demultiplexer, wavelength-selective splitter and active tunable splitter.

2. Theoretical and numerical analysis of MMI effect in MIM waveguides

As shown in the inset of Fig. 1(a), the fundamental structure of the MIM waveguides consists of an insulator layer (air) symmetrically sandwiched between metal (silver) layers. When excited with transverse magnetic field (H_y), the complex propagation constants β_m of the TM_m modes can be solved by [12]

$$\kappa_1 w = m\pi + 2\arctan(\frac{\varepsilon_1 \alpha_2}{\varepsilon_2 \kappa_1}) \quad \text{with} \quad m = 0,\ 1,\ 2...... \tag{1}$$

where $\kappa_1 = (k_0^2 \varepsilon_1 - \beta_m^2)^{1/2}$, $\alpha_2 = (\beta_m^2 - k_0^2 \varepsilon_2)^{1/2}$, $k_0 = 2\pi / \lambda$, w is the waveguide width and ε_1, ε_2 are the dielectric constants of air ($\varepsilon_1 = 1$) and silver, respectively. The wavelength-dependent complex dielectric constants of silver are taken from the measured values in Ref [13]. Figure 1 illustrates the dispersion relation of the first four TM modes [Fig. 1(a)] and the corresponding mode profiles [Fig. 1(b)] at the wavelength of $\lambda = 1.55\mu m$. It can be seen that for a given wavelength, the fundamental TM_0 mode does not exhibit a cutoff, but the number of modes supported by the waveguide increases with the width w. Moreover, as a typical feature of surface plasmon, all the modes have a clear amplitude enhancement at the air/silver boundaries, and exponentially decay towards the silver side. Through this paper the field in the multimode region are launched from single mode input MIM waveguides with a width of $w_s = 100nm$. It should be noted that if the input position falls on the zero field point of a certain mode, the mode will not be excited [8]. This property can be utilized to control the interference pattern in the multimode waveguides.
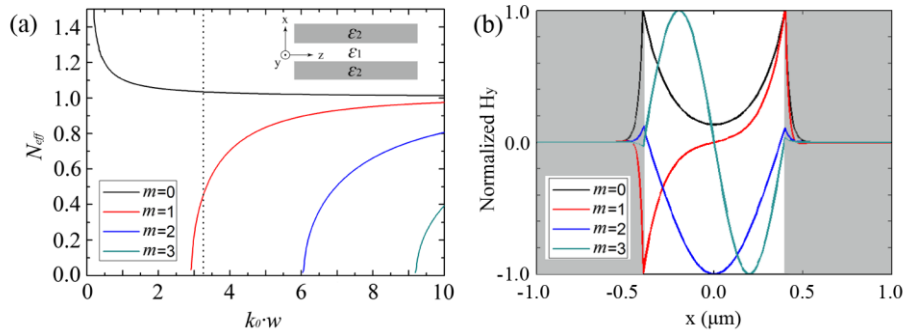
Fig. 1. (a) The dispersion relation of the MIM waveguides (shown in the inset). (b) The field profile of the first four TM modes in a 0.8μm-wide waveguide.

According to the self-imaging principle that is well known for conventional dielectric waveguides [8], the excited modes in a multimode waveguide will interfere with each other due to their different propagation constants, and the interference pattern can be characteristic by the beat length $L_\pi = \pi / (\beta_0 - \beta_1)$. In order to examine the theory for the MIM waveguides, we investigate the interference between the TM_0 and TM_1 modes. At $\lambda = 1.55$μm, the cutoff widths for TM_1, TM_2 and TM_3 mode is 0.72μm, 1.50μm and 2.27μm, respectively. So, for a multimode waveguide with width $w_m = 0.8$μm [dashed line in Fig. 1(a)], the theoretical propagation constants of TM_0 and TM_1 mode are calculated to be $\beta_0 = 4.194$μm^{-1} and $\beta_1 = 1.799$μm^{-1}, corresponding to $L_\pi^{1.55} = 1.312$μm. To compare with the theoretical results we implement FEM simulation and observe the interference pattern [Fig. 2(a)]. The waveguide length L is assumed to be infinite, and the input field is asymmetrically launched into the multimode waveguide for the purpose of efficiently exciting the TM_1 mode. Owing to the MMI effect, the power couples to the opposite side of the waveguide after each beat length and form a repetitive field distribution. The averaged beat length taken from the numerical result is 1.31μm, agrees with the theoretical prediction. For $\lambda = 1.31$μm, the theoretical and simulated beat length is 1.828μm and 1.83μm, respectively. In addition, we observe the MMI effect in wider waveguides [Fig. 2(b) and 2(c)]. With specific input position, their interference pattern can also be understood by the beating of the excited modes. Then, in the following sections, we will use the self-imaging principle to guide the design of plasmonic MMI devices.
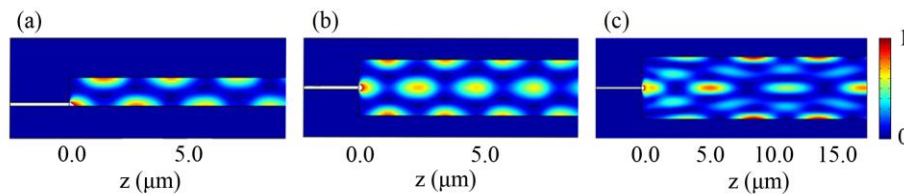

Fig. 2. The time-averaged poynting vector distribution in the multimode waveguides. The width of the waveguide is (a) $w_m = 0.8$μm, (b) $w_m = 1.6$μm and (c) $w_m = 4$μm.

3. Design of plasmonic MMI devices in MIM waveguides

3.1 Demultiplexer based on 1 × 2 configuration

In this section, we propose a wavelength demultiplexer using the MMI effect. As an example, here we aim at separating 1.55μm and 1.31μm incident light. The structure is identical to the

previous model in Fig. 2(a) except that two single mode output waveguides (w_s = 100nm) are connected to the end of the multimode region (w_m = 0.8μm). To separately rout the two wavelengths into different output waveguides, the length of the multimode region L should satisfies

$$(k+1)L_\pi^{1.55} \approx kL_\pi^{1.31} \qquad (2)$$

where k is a positive integer. Based on the previous results, the minimum integer to approximately meet the equation is k = 3, corresponding to $L \approx 5.37$μm. However, with a finite L, the slight field distortion caused by reflection at the end of the multimode waveguide must be considered. According to the simulation results, the length is further optimized to L = 5.17μm in order to achieve the best extinction ratio for both wavelengths. Figure 3 shows the simulated magnetic field intensity in the optimized structure. The extinction ratio for the λ = 1.55μm wave and λ = 1.31μm wave is 11.6 dB and 11.4 dB, respectively while the total energy loss, which comes from the absorption in silver and the coupling loss between the single mode and multimode waveguides, are ~1.2 dB for λ = 1.55μm wave and ~0.9 dB for λ = 1.31μm wave. The reflection at the waveguide junctions and the ends of the multimode region induces the standing-wave pattern in the input access waveguides and limits the total transmittance. Usually the reflection could be reduced by adding taper structures.
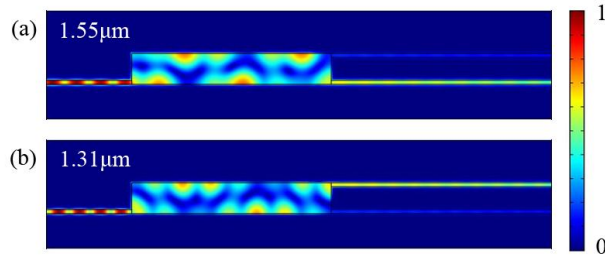

Fig. 3. The magnetic field intensity $|H_y|$ in the MMI demultiplexer at the wavelength of (a) λ = 1.55μm and (b) λ = 1.31μm.

3.2 Wavelength-selective splitter based on 3 × 3 configuration

Another important element for the integrated circuits is beam splitters. Although T-type or Y-type splitters composed of single mode MIM waveguide have rather low bending loss [14], a limitation is that they can only have equal split effect for all the wavelengths. Here we purpose a wavelength-selective splitter using the MMI effect. Our goal is to separate one wavelength into two equal parts while maintain another one unseparated. As shown in Fig. 4, the device configuration is based on a symmetric 3 × 3 coupler where the incident light is launched from the left single mode waveguides and output through the right ones. The width of the multimode waveguide (w_m = 1.6μm) guarantees the first three TM modes are supported at both λ = 1.55μm and λ = 1.31μm. If the field is launched from the central port B [see Fig. 4(a)], the TM_1 mode will not exist due to its anti-symmetric profile. In this case the interference is decided by the TM_0 and TM_2 modes and therefore the beat length should be given by $L_\pi = \pi/(\beta_0 - \beta_2)$. For λ = 1.55μm/1.31μm, we have L_π = 1.177μm/1.663μm, agrees well with the numerical simulation [Fig. 2(b)].

Similar to the previous analysis, we need a proper length L of the multimode waveguide to selectively route the wavelengths. Based on Eq. (2), the minimum length that meets the requirement is found to be L = 3.2μm, corresponding to k = 2. Figure 4 illustrates the magnetic field intensity in the structure, where the λ = 1.55μm wave is equally split into output port 1 and 3 [Fig. 4(a)] while the λ = 1.31μm wave directly transmits through port 2 [Fig. 4(b)]. The weak field appears in the unexcited input waveguides come from the

reflection at the right side of the multimode region. Table 1 summarizes the transmittance (defining as the output power normalized to the total input power) at each output port. One can see that for the wavelength of $\lambda = 1.55\mu m$ and $\lambda = 1.31\mu m$, the extinction ratio is 18.7 dB and 30.2 dB, respectively, and the total insertion loss is found to be ~2.2 dB ($\lambda = 1.55\mu m$) and ~0.8 dB ($\lambda = 1.31\mu m$). The larger loss for $\lambda = 1.55\mu m$ wave is because more energy escape from the unexcited input waveguides (port A&C).

As an opposite situation, if the field is symmetrically launched from port A&C, the TM_1 mode can be excited but will destructively interference with itself. As a result, the beat length L_π remains unchanged. This can be verified from Fig. 4(c) and 4(d), where the $\lambda = 1.55\mu m$ wave couples into the central port 2, but the $\lambda = 1.31\mu m$ wave still transmits through the side ones. The power transmittance is also shown in Table 1.
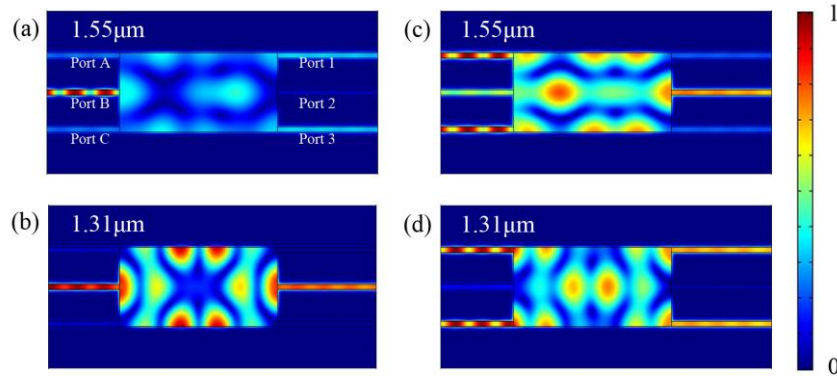

Fig. 4. The magnetic field intensity $|H_y|$ in the 3×3 coupler structure when light is (a)-(b) centre-launched from port B or (c)-(d) symmetrically launched from port A&C.

Table 1. The transmittance at the three output ports of the 3×3 coupler

wavelength	Input at port B			Input at port A&C		
	Output port 1	Output port 2	Output port 3	Output port 1	Output port 2	Output port 3
1.55μm	29.7%	0.8%	29.7%	4.1%	52.9%	4.1%
1.31μm	0.04%	83.6%	0.04%	44.5%	1.1%	44.5%

3.3 Towards active tunable splitters

Finally, based on the previous discussion, we consider a tunable splitter whose power distribution at the output ports is controlled by refractive index modulation in the multimode region. The modulation can usually be achieved with the help of nonlinear materials, such as electro-optical materials with a large electro-optic coefficient [15,16].

As shown in Fig. 5, the splitter is constituted by a lateral symmetrical 1×3 coupler with structural parameters $w_m = 1.1\mu m$ and $L = 11\mu m$. It is assumed that the insulator layer of the multimode waveguide is filled with materials whose refractive index can be tuned actively, and the initial index is set as $n = 1.5$. Under this configuration, the interference pattern still depends on the TM_0 and TM_2 modes. Since Eq. (1) and (2) imply that the beat length can be changed by tuning the refractive index n, we can expect to control the power distribution at the different output ports in this way. Figure 5(a)–5(c) illustrate the magnetic field intensity in the structure as the incident light with a wavelength of $\lambda = 1.55\mu m$ is launched from the left input waveguide. When n equals to 1.5, 1.472 and 1.458, the structure functions as a 1×1, 1×3 and 1×2 splitter, respectively, and the corresponding transmittance is summarized in Table 2. The total loss of the device is over 3 dB, which can be improved by structure optimization (e. g. adding tapper structure at the waveguide junctions). It is worth noting that

the required modulation on the refractive index exceeds the maximum change in the refractive index of most electrooptic media, which are usually at the order of 10^{-3}. However, several kinds of materials with ultralarge electro-optic coefficients (larger than 150pm/V) have also been obtained in the recent years [15,16]. With the development of such materials, the required index-modulation in our device (~0.05) could be achieved with an external voltage lower than 100V.
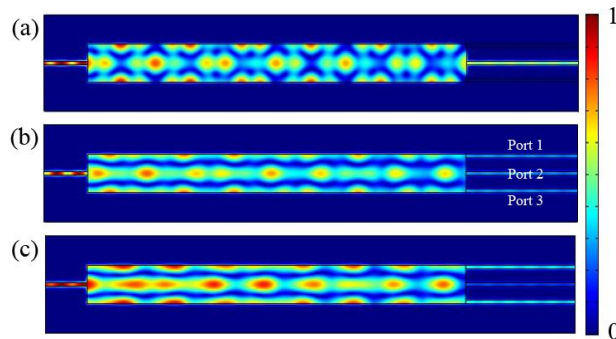

Fig. 5. The magnetic field intensity $|H_y|$ in the MMI tunable splitter at the wavelength of $\lambda = 1.55\mu m$. The refractive index in the multimode region is (a) $n = 1.5$, (b) $n = 1.472$ and (c) $n = 1.458$.

Table 2. The transmittance at the three output ports of the tunable splitter

Refractive index	Output port 1	Output port 2	Output port 3
$n = 1.5$	0.04%	49.5%	0.04%
$n = 1.472$	15.2%	15.2%	15.2%
$n = 1.458$	20.1%	4.8%	20.1%

4. Conclusion

In conclusion, we have theoretically and numerically investigated the MMI effect in multimode MIM waveguides. We demonstrated that the MMI effect can be utilized to design wavelength-selective devices with high extinction ratio or active controllable devices by refractive index modulation. Considering the strong confinement ability of the MIM waveguides and the compact size of the proposed structures, it may find application in high-density photonic integration.